Determination of absolute thermal rate constants for the charge-transfer reaction $DBr^+(^2\Pi_i, v^+) + HBr \rightarrow HBr^+(^2\Pi_{i'}, v'^+) + DBr$

Jinchun Xie and Richard N. Zare
Department of Chemistry, Stanford University, Stanford, California 94305-5080

(Received 10 September 1991; accepted 29 November 1991)

The charge-transfer reaction $DBr^+(^2\Pi_i, v^+, J^+) + HBr \rightarrow HBr^+(^2\Pi_{i'}, v'^+, J'^+) + DBr$ is studied in a state-to-state manner under thermal conditions in a slowly flowing gas mixture of HBr and DBr. The DBr^+ reagent is prepared in a selected vibronic level by using $(2+1)$ resonance-enhanced multiphoton ionization. The HBr^+ product is detected in a quantum-state-specific manner using laser-induced fluorescence. From the measurements of the molecular density and the populations of both HBr^+ product and DBr^+ reagent, the absolute thermal rate constants $k(i, v^+ \rightarrow i', v'^+)$ are determined for this charge-transfer process. The rate constants for near-resonant charge transfer in which $\Delta v^+ = 0$ and $\Delta i = 0$ are much larger than charge-transfer channels in which either $\Delta i \neq 0$ or $\Delta v^+ \neq 0$; the smallest rate constants are for those channels in which both $\Delta i \neq 0$ and $\Delta v^+ \neq 0$. The rotational distribution of the $HBr^+(i', v'^+)$ product fits a temperature well in each case. For near-resonant charge transfer, the rotational temperature is slightly warmer than thermal, whereas for nonresonant charge transfer, the rotational temperature is much hotter than thermal. A model in which the excess energy of a charge-transfer process is statistically partitioned among all the degrees of freedom of the complex is able to predict closely the observed rotational temperature.

I. INTRODUCTION

One of the major themes of reaction dynamics is state-to-state chemistry in which the reactants are prepared in a limited number of known quantum states and the collisionally unrelaxed products are analyzed for their resulting internal state distributions.[1,2] Such information provides deep insight into the reaction mechanism, such as the special role possibly played by different motions (energy modes) in the reaction complex and the partitioning of the total energy available among the different degrees of freedom in the products. Much progress in state-to-state dynamics has been recently reported for neutral–neutral reactions, such as $F + H_2(v=0, J=1,3) \rightarrow HF(v', J') + H$ (Ref. 3), $O + HCl(v=2, J) \rightarrow OH(v', J') + Cl$ (Ref. 4) $Ca + HF(v=1, J) \rightarrow CaF(v', J') + H$ (Ref. 5), and $D + H_2(v=1, J=1) \rightarrow HD(v'=1, J') + H$ (Ref. 6). Detailed information of a similar type has been lacking, in general, for ion–molecule reactions, although recent advances[7–9] in the state preparation and state detection of ions promise to close this gap.

The pioneering one-photon ionization experiments of Chupka and co-workers[10] demonstrated that ions can be prepared in selected internal states. Of particular interest is the use of resonance-enhanced multiphoton ionization (REMPI) to create reagent ions in a single selected vibrational level with a limited number of rotational levels.[11,12] It is also possible to quantify the internal state populations of the product of an ion–molecule reaction using laser-induced fluorescence (LIF),[13] as illustrated by Leone and co-workers for the charge-transfer reactions $Ar^+ + N_2 \rightarrow Ar + N_2^+$ (Ref. 14) and $Ar^+ + CO \rightarrow Ar + CO^+$ (Ref. 15).

Most ion–molecule reactions are carried out under hyperthermal collision energies where the ions are accelerated in an external electric field, such as in crossed ion beam experiments, in drift tubes, and in flowing afterglow studies.[16] Alternatively, ion–molecule reactions can be studied at very low collision energies using ion traps[9,17] and supersonic expansions.[18] We report here the state-to-state study of thermal ion–molecule reactions carried out in a bulb. Single-collision conditions are established by setting the time delay between ion state creation and product ion state detection using laser techniques. By determining the densities of the reagents, we can put these state-to-state measurements on an absolute basis, i.e., we can determine thermal state-to-state absolute rate constants for the charge-transfer reaction $DBr^+ + HBr \rightarrow HBr^+ + DBr$. In this experiment the DBr^+ is prepared in a selected vibronic state by $(2+1)$ REMPI and the internal state distribution of the HBr^+ product is analyzed using laser-induced fluorescence.

We believe that this method for studying thermal ion–molecule reactions under bulb conditions is limited to small molecules for which it is possible to prepare the ion in a state-selective manner using REMPI and to probe the reaction product using LIF. Although restricted in scope to such reaction systems, the information made available from such studies is quite detailed. This technique should be applicable to a wide range of ion–molecule reaction systems in various pressure regimes.

II. EXPERIMENT

Figure 1 shows the experimental setup, consisting of a reaction chamber, two laser light sources, and a signal detection system with associated timing controllers. Figure 2 illustrates the timing sequence. First the REMPI laser is fired to generate DBr^+ ions in the reaction chamber, which is

Downloaded 23 Feb 2012 to 171.64.124.19. Redistribution subject to AIP license or copyright; see http://jcp.aip.org/about/rights_and_permissions

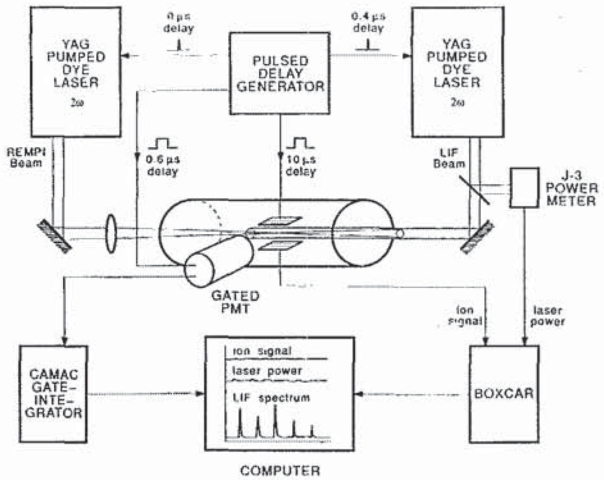

FIG. 1. Schematic diagram of the experimental setup, which includes the REMPI and LIF laser systems, a reaction cell, the detectors (gated photomultiplier, electrode plates, and laser power meter), timing controller, and data acquisition electronics.

filled with a 1:2 mixture of DBr to HBr at a total pressure of 15 mTorr. Then, the LIF laser is fired to detect both DBr^+ and HBr^+ ions in a quantum-state-specific manner. The time delay is 400 ns, so that fewer than one in five DBr^+ ions have made a single collision. The photomultiplier is gated so that it is opened to detect fluorescence only after the LIF

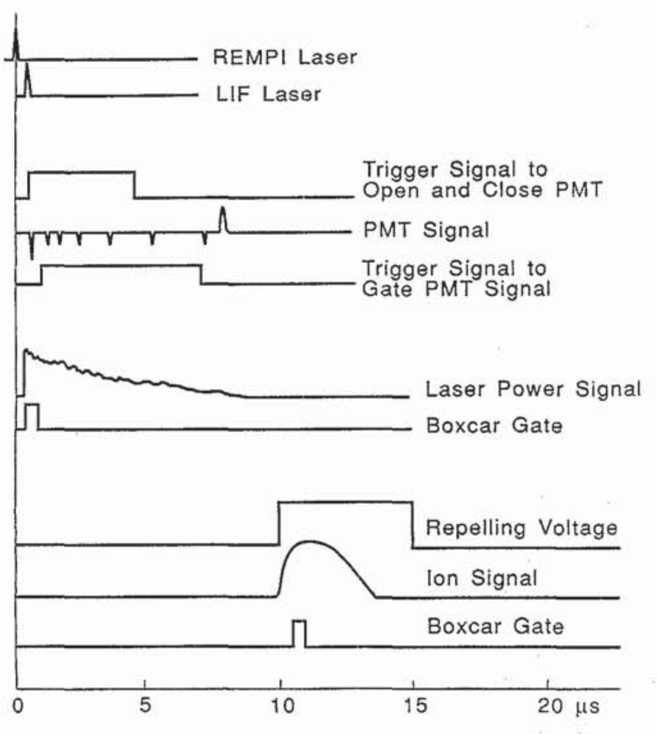

FIG. 2. Timing of the pulse sequence for REMPI and LIF lasers; the triggering of the photomultiplier (PMT); the triggering of the photomultiplier signal integrator; the boxcar gate for the laser power meter; the repeller voltage; and the boxcar gate of the integrator of the ion signal. Note the spurious spikes introduced in the PMT signal by the opening and closing of the gating voltage to the first dynode.

laser pulse. In addition, LIF laser power is recorded using a pyroelectric detector and the number of ions is also measured by applying a delayed pulse voltage to the repeller plate. By normalizing the fluorescence signal to laser power and ion production, we determine the absolute thermal rate constant for the charge-transfer process from a prepared level of DBr^+ to various levels of HBr^+.

The reaction chamber has been equipped with Brewster's angle windows, glass Wood's horns, and baffle arms to eliminate scattered light. The baffles are made of 0.001 in. thick shims of stainless steel, each one having a sharp orifice. The shims are blackened by oxidation. The fluorescence is collected by a 2 in. diameter f_1 lens system and a spherical mirror on the opposite side. The lenses, mounted in a tube with a 25×7 mm opening pointed toward the laser focal region, image the fluorescence onto a 12×12 mm cathode of the photomultiplier. A filter system, consisting of a longpass filter (WG345, Oriel) and shortpass filter (UG11, Oriel), is placed immediately in front of the photomultiplier. This filter system isolates the (0,0) and (0,1) bands of $A\,^2\Sigma^+-^2\Pi_{3/2}$ and the (0,0) band of $A\,^2\Sigma^+-^2\Pi_{1/2}$ for the DBr^+ and HBr^+ fluorescence. The filter system is centered at 357 nm with a FWHM of 17 nm. The transmission profile is nearly Gaussian with a transmission coefficient of 0.45 at its maximum.

When no gases are flowing, the stainless-steel chamber is pumped down to 1×10^{-7} Torr, using a 3 in. diffusion pump (EO2, Edwards) through a liquid nitrogen trap. The DBr (99% Deuterium purity, Cambridge Isotope Co.) and HBr (99.7% chemical purity, Matheson) gases slowly flow through the reaction chamber. The sample pressure is monitored by a capacitance manometer (Model 122A, MKS Instruments, Inc.) and maintained constant. The flow has been regulated carefully so that virtually no pressure difference exists within the chamber. Pure HBr is obtained from the high-pressure HBr cylinder by evaporation of the liquid HBr. Pure DBr cannot be obtained from the DBr lecture bottle in the same manner because the pressure is too low in the lecture bottle to liquefy the DBr. Instead, we cool the DBr lecture bottle in liquid nitrogen and pump away any D_2. Then we place the DBr lecture bottle in Dry Ice, which prevents the escape of any Br_2. The gas lines are regularly pumped below 1 mTorr during bake out. During an experimental run, the flowing gases are frozen out using a demountable liquid nitrogen trap in the foreline.

The REMPI laser beam is generated as follows. The third harmonic of a Nd:YAG laser (GCR-3, Spectra-Physics) pumps a dye laser (PDL-3, Spectra-Physics) containing coumarin 500 (540–480 nm). The output is frequency doubled using an autotracker (WEX-1, QuantaRay) with 83° KD*P (270–260 nm) and 55° BBO (260–240 nm) crystals. The resulting beam has typically 5–10 mJ of uv output with a linewidth of 0.08 cm^{-1} in the wavelength range 270–253 nm. Another laser system consisting of a Nd:YAG laser (DCR-1, QuantaRay), a dye laser (PDL-1, QuantaRay), a doubling autotracker (WEX-1, QuantaRay), and a H_2 Raman cell is used to generate the LIF probe beam in the wavelength range 350–380 nm. We iris the beam to a 5 mm diameter spot size having a pulse energy of about 50 μJ. The low

Downloaded 23 Feb 2012 to 171.64.124.19. Redistribution subject to AIP license or copyright; see http://jcp.aip.org/about/rights_and_permissions

power is necessary to avoid saturation.

We use a photomultiplier tube (R943-02, Hamamatsu) with a gated D-type socket assembly (C1392-02, Hamamatsu) to detect the fluorescence. A 250 V gate is applied between the cathode and the first dynode to block photoelectrons when the gate is off and to attract the photoelectrons when the gate is on. A TTL pulse (6 μs wide, delayed by 0.4 μs) triggers the 250 V gate and opens an 8 μs wide gate delayed by 0.9 μs on the output of the photomultiplier. The off–on switching ratio of $1:10^4$ helps to reject the early-time, strong emission background resulting from radiative decay of the intermediate state of DBr excited in the $(2+1)$ REMPI process. The fluorescence signal is integrated with a 6 μs gate delayed by 1 μs using an AD converter (2249W, LeCroy) and a gate-delay generator (2323A, LeCroy). A pyroelectric detector (J3-09, Molectron) monitors the LIF laser pulse energy from a beam splitter. The pulsed output from the pyroelectric detector is gated using a boxcar integrator (165, PAR). A pair of plates are placed above and below the ionization region, one of which is pulsed (6 μs width, delayed by 10 μs and ~ 30 V amplitude) to repel ions to the other plate. The ion signal from the collector plate is gated at a delay of 11 μs and detected using another channel of the boxcar integrator. The dc outputs of the boxcar are digitized via an AD converter and transferred into a microcomputer (PC/XT, IBM) together with the LIF signal under CAMAC control. The three signals are recorded for each laser shot and averaged over 20 shots at each step of the LIF scan.

III. RESULTS AND ANALYSIS

A. Reagent state preparation

The DBr^+ reagent is prepared in a small number of internal states using $(2+1)$ REMPI via the $F\,^1\Delta_2$ and $f\,^3\Delta_2$ Rydberg states of DBr. We denote the fine-structure level of the DBr^+ $X\,^2\Pi$ state by i, where $i=\frac{1}{2}$ or $\frac{3}{2}$. The rovibronic level of the ion is denoted by v^+, J^+. Hence the internal state is labeled by (i,v^+,J^+). Once DBr^+ is produced, the internal-state distribution is determined by LIF via the transition DBr^+ $A\,^2\Sigma^+$–$X\,^2\Pi_i$. These measurements are also supplemented by time-of-flight photoelectron spectroscopy,[19] which has sufficient resolution to confirm the assignments of i and v^+ but not J^+.

Table I lists the degree of selection for i and v^+. We find that the reagent ion can be prepared in an almost pure (i,v^+) state. As expected from previous work,[20] the vibrational level of the intermediate state becomes the same vibrational level of the ion state because of the Franck–Condon principle applied to potential curves of similar shapes. Another feature is the almost complete selection of the fine-structure component i. Evidently, the ionic core of the intermediate Rydberg state follows closely Hund's case (c) coupling, and the photoionization step removes the Rydberg electron without disturbing the ionic core. As Table I shows, this explanation would account for the strong selection of i. We suspect that this selection mechanism is general for photoionization of all intermediate states obeying Hund's case (c) coupling. Additional evidence for this behavior is the work of Koenders *et al.*,[21] who demonstrated the photoselection of Br_2^+ $^2\Pi_{1/2}$ or $^2\Pi_{3/2}$ in the $(2+1)$ REMPI of Br_2.

The rotational distribution created in the DBr^+ reagent ion is limited to a few levels distributed about the J value of the intermediate state selected because only a small number of photoelectron partial waves contribute to the ionization process.[22] This conclusion is borne out by Fig. 3, which shows the DBr^+ rotational distribution resulting from excitation of the $P(3)$ line of the DBr $F\,^1\Delta_2$–$X\,^1\Sigma^+$ (0,0) band. The labels $+$ and $-$ denote the total parity of the DBr^+ rovibronic level. For this particular transition the $+$ parity levels are favored over the $-$ parity levels by 4:1. The $+$ and $-$ parity levels with the same J^+ value correspond to the different Λ components (Ω components) of the same rotational level. In the spectroscopic literature the levels with $+(-1)^{J^+-1/2}$ parity are called e levels, those with $-(-1)^{J^+-1/2}$ parity are called f levels.[23] More information about the details of the reagent ion rotational distribution may be found elsewhere.[24]

In a mixture of DBr and HBr, the transitions of the two isotopomers overlap, especially for the (0,0) band of the F–X and f–X transitions. Figure 4 illustrates this behavior for a 2:1 mixture of HBr to DBr. Because DBr has approximately twice as many lines as HBr in the same wavelength interval, arising from the half-as-large rotational constant of DBr compared to HBr, it is easier to find isolated DBr lines than HBr lines. Although some DBr lines appear to be separated from HBr lines, closer inspection shows that the wings of the HBr lines may overlap the DBr lines causing some HBr^+ formation along with DBr^+ formation. We found that only a few DBr^+ lines, such as $P(3)$ and $S(7)$, produce DBr^+ without detectable HBr^+ contamination.

Figure 5 demonstrates the absence of HBr^+ at early times when the $P(3)$ line of the DBr F–X (0,0) band is excited. At a delay of 20 ns the LIF spectrum shows no HBr^+,

TABLE I. Spin–orbit and vibration state selection and preparation of reagent DBr^+.

Ionic state	Selectivity	Intermediate state	Transition	Two-photon Wavelength (nm)
$^2\Pi_{1/2}, v^+=1$	98%	$F\,^1\Delta_2\,[^2\Pi_{1/2}]5p\pi, v=1$	$R(2)$	253.958
$^2\Pi_{1/2}, v^+=0$	99%	$F\,^1\Delta_2\,[^2\Pi_{1/2}]5p\pi, v=0$	$P(3)$	259.583
$^2\Pi_{3/2}, v^+=1$	98%	$f\,^3\Delta_2\,[^2\Pi_{3/2}]5p\pi, v=1$	$R(1)$	263.304
$^2\Pi_{3/2}, v^+=0$	99%	$f\,^3\Delta_2\,[^2\Pi_{3/2}]5p\pi, v=0$	$R(1)$	269.182

Downloaded 23 Feb 2012 to 171.64.124.19. Redistribution subject to AIP license or copyright; see http://jcp.aip.org/about/rights_and_permissions

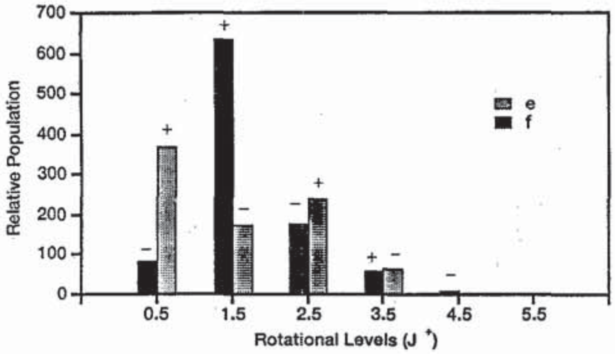

FIG. 3. Rotational population distribution of the reagent ion DBr^+ ($^2\Pi_{1/2}, v^+ = 0$) produced by (2 + 1) REMPI via the $P(3)$ line of the $F\,^1\Delta_2$–$X\,^1\Sigma^+$ (0,0) band.

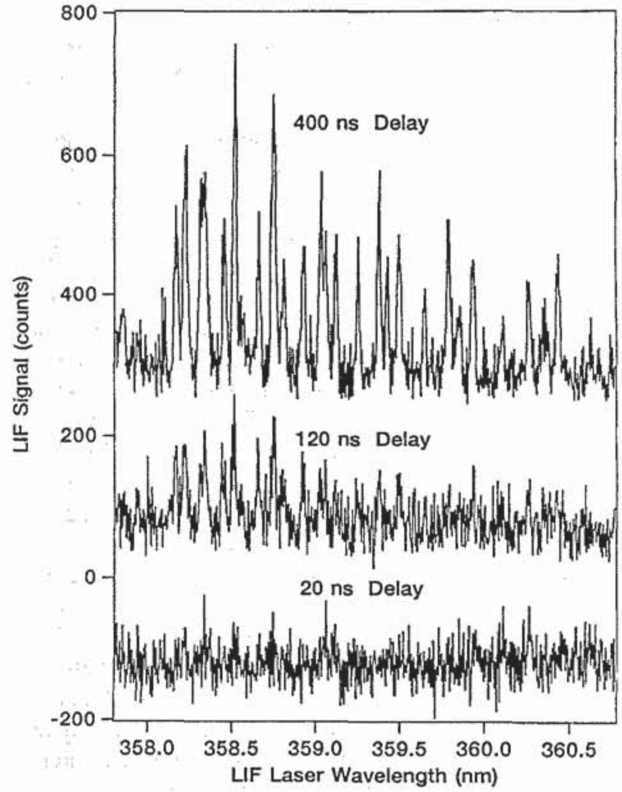

FIG. 5. LIF spectra of the HBr^+ $A\,^2\Sigma^+$–$^2\Pi_{1/2}$ (1,0) band recorded under different time delays between the REMPI laser pulse and the LIF laser pulse.

whereas at a delay of 400 ns HBr^+ is clearly apparent, formed by the charge-transfer reaction $DBr^+ + HBr \rightarrow HBr^+ + DBr$.

Finally, we note that the production of Br^+ and/or D^+ (H^+) appears to be negligible under our operating conditions. Mass spectrometry has shown that no ionic fragments occur in the (2 + 1) REMPI of HBr via the $f\,^3\Delta_2$ state and less than a few percent via the $v = 1$ level of the $F\,^1\Delta_2$ state at higher laser powers than we employed.[25] Consequently, we attribute all HBr^+ production as arising from charge transfer of HBr with DBr^+.

B. Product state distributions

Figure 6 shows a typical LIF spectrum of HBr recorded in a 2:1 mixture of HBr to DBr at a total pressure of 15 mTorr. The DBr^+ reagent ion is produced by (2 + 1) REMPI via the $P(3)$ line of the F–X (0,0) band and the HBr^+ ion is detected by LIF after a 400 ns delay using the HBr^+ $A\,^2\Sigma^+$–$X\,^2\Pi_{1/2}$ (0,0) band. The good signal-to-noise ratio of the lines allows the assignment of the intense R_{12}, Q_2, Q_{12}, and P_2 branch members. Members of the P_{12} and R_2 satellite branches are too weak to be identified.

Rotational distributions are determined by integrating the intensity of a line normalized to the probe laser power and to the total amount of ions formed. The integrated intensity is then divided by an appropriate rotational line strength

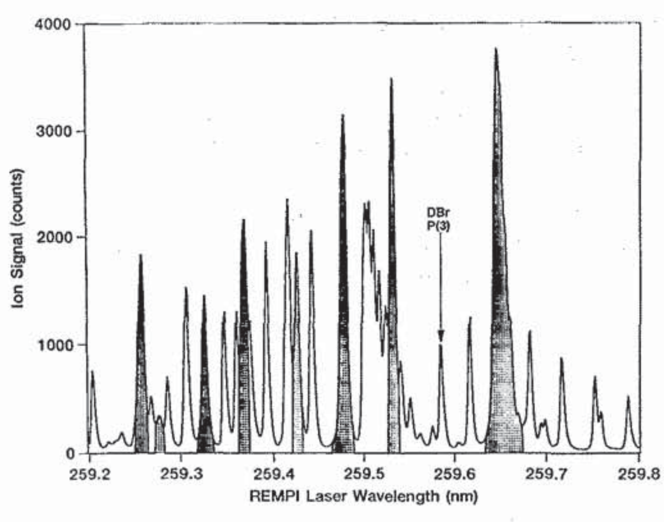

FIG. 4. (2 + 1) REMPI spectrum of DBr and HBr $F\,^1\Delta_2$–$X\,^1\Sigma^+$ (0,0) band recorded in a 1:2 mixture of DBr to HBr at a total pressure of 15 mTorr. The HBr lines have been shaded. The isolated DBr $P(3)$ line is indicated.

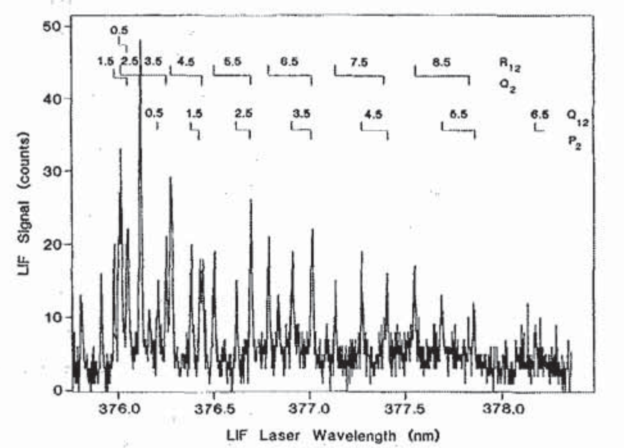

FIG. 6. LIF spectrum of the HBr^+ $A\,^2\Sigma^+$–$^2\Pi_{1/2}$ (0,0) band. The HBr^+ ions are produced from the charge-transfer reaction between DBr^+ ($^2\Pi_{1/2}, v = 0$) and HBr. The assignments of the rotational lines of the R_{12}, Q_2, Q_{12}, and P_2 branches are indicated.

Downloaded 23 Feb 2012 to 171.64.124.19. Redistribution subject to AIP license or copyright; see http://jcp.aip.org/about/rights_and_permissions

factor. For the $A\,^2\Sigma^+ - X\,^2\Pi_{1/2}$ transition, we use the Hund's case (c) line strength for a $\frac{1}{2}\rightarrow\frac{1}{2}$ transition[26] and for the $A\,^2\Sigma^+ - X\,^2\Pi_{3/2}$ transition we use standard formulas,[27] where $\mu_\parallel = 0.399$[24] and $Y = -333.32$.[28] Care is taken to avoid saturation effects, which could be verified by changing the probe laser power by a factor of 3. Each line intensity is an average of three scans, and the spectrum has been corrected for the change in fluorescence detection efficiency with excitation wavelength caused by the wavelength-dependent response of the filter–photomultiplier combination. This correction is approximately 10% in going from low to high J^+. A final correction is made for polarization effects by simply adding together the P, Q, and R branch members with the same J^+ quantum number. This last correction is not exact but introduces little error, especially for higher J^+ values.

Figures 7–10 present the resulting HBr^+ rotational population distributions for charge transfer from $DBr^+(i=\frac{1}{2}, v^+=0)$ (Fig. 7), $DBr^+(i=\frac{1}{2}, v^+=1)$ (Fig. 8), $DBr^+(i=\frac{3}{2}, v^+=0)$ (Fig. 9), and $DBr^+(i=\frac{3}{2}, v^+=1)$ (Fig. 10). In most cases, an individual rotational population in each distribution has a typical error bar of $\pm 10\%$ (one standard deviation). Exceptions are the weaker charge-transfer channels $DBr^+(\frac{1}{2},1)\rightarrow HBr^+(\frac{1}{2},0)$ and $DBr^+(\frac{1}{2},0)\rightarrow HBr^+(\frac{3}{2},1)$, for which the error bars are 30% and 60%, respectively. The charge-transfer channel $DBr^+(\frac{1}{2},1)\rightarrow HBr^+(\frac{3}{2},1)$ was not measured because the signal-to-noise ratio was so poor.

Note that the rotational population distributions are smooth, i.e., slowly varying as a function of J^+. The near-resonant charge-transfer channels $DBr^+(\frac{1}{2},0)\rightarrow HBr^+(\frac{1}{2},0)$ [Fig. 7(a)] and $DBr^+(\frac{3}{2},0)\rightarrow HBr^+(\frac{3}{2},0)$ (Fig. 9) have rotational distributions that are similar to the rotational distribution of the HBr reagent at room temperature, whereas the nonresonant channels [Figs. 7(b), 7(c), 8, and 10) show rotational distributions that are hotter. Thus, in all cases, the J^+ distribution of the HBr^+ product differs markedly from

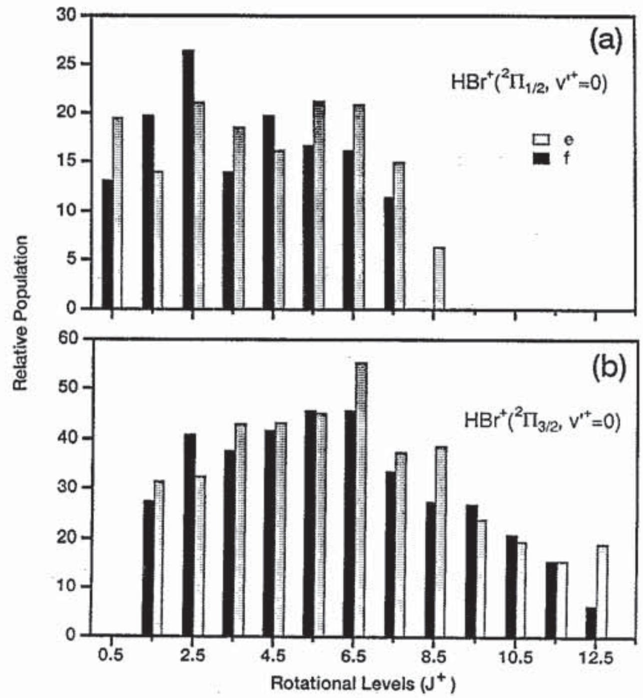

FIG. 8. Product HBr^+ rotational population distributions from the reaction $DBr^+(^2\Pi_{1/2}, v^+=1)$ + HBr for (a) $HBr^+(^2\Pi_{1/2}, v'^+=0)$ and (b) $HBr^+(^2\Pi_{3/2}, v'^+=0)$.

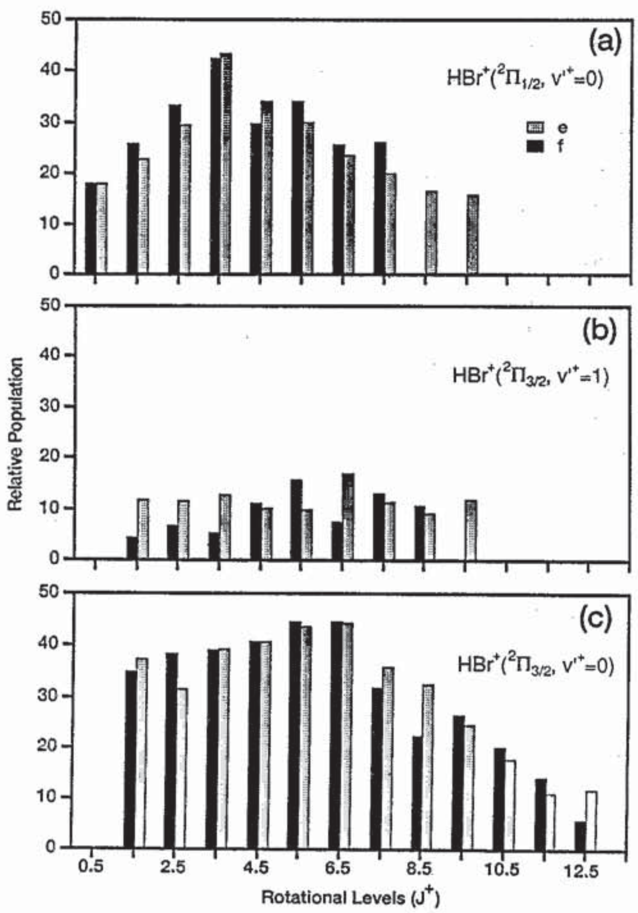

FIG. 7. Product HBr^+ rotational population distributions from the reaction $DBr^+(^2\Pi_{1/2}, v^+=0)$ + HBr for (a) $HBr^+(^2\Pi_{1/2}, v'^+=0)$, (b) $HBr^+(^2\Pi_{3/2}, v'^+=1)$, and (c) $HBr^+(^2\Pi_{3/2}, v'^+=0)$.

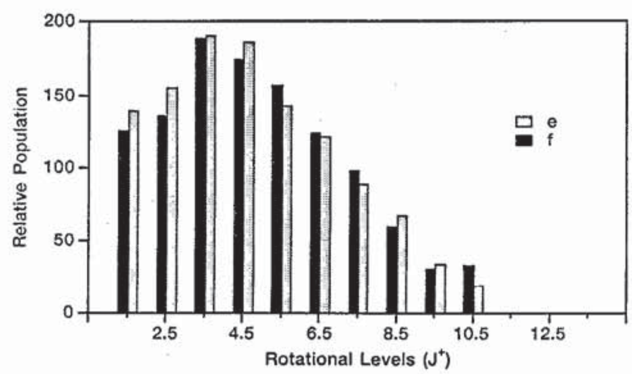

FIG. 9. Product $HBr^+(^2\Pi_{3/2}, v'^+=0)$ rotational population distribution from the reaction $DBr^+(^2\Pi_{3/2}, v^+=0)$ + HBr.

Downloaded 23 Feb 2012 to 171.64.124.19. Redistribution subject to AIP license or copyright; see http://jcp.aip.org/about/rights_and_permissions

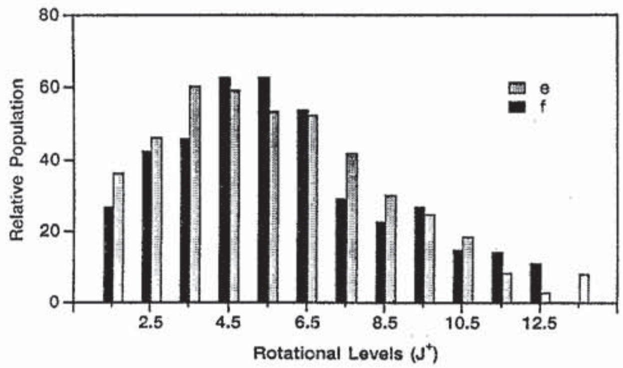

FIG. 10. Product HBr^+ ($^2\Pi_{3/2}, v'^+ = 0$) rotational population distribution from the reaction DBr^+ ($^2\Pi_{3/2}, v^+ = 1$) + HBr.

the narrow J^+ distribution of the DBr^+ reagent (see Fig. 3). In almost all cases, the populations of the + and − parity levels with the same J^+ value are nearly equal in the HBr^+ product ion, again in sharp contrast to the populations of the + and − parity levels in the DBr^+ reagent ion.
− parity levels in the DBr^+ reagent ion.

Boltzmann plots are prepared by graphing the rotational population, divided by the rotational degeneracy factor $(2J^+ + 1)$, vs rotational energy (see Fig. 11). We find that the Boltzmann plot for HBr^+ ($i' = \frac{3}{2}, v'^+ = 0$) from the reaction DBr^+ ($i = \frac{3}{2}, v^+ = 0$) + HBr is linear [see Fig. 11(a)], whereas that for HBr^+ ($i' = \frac{3}{2}, v'^+ = 0$) from the reaction DBr^+ ($i = \frac{1}{2}, v^+ = 0$) + HBr is almost linear [see Fig. 11(b)]. Thus the rotational population distributions are well described by temperatures. In Table II we list the rotational temperatures of the HBr^+ product ion for the different energy-transfer channels studied.

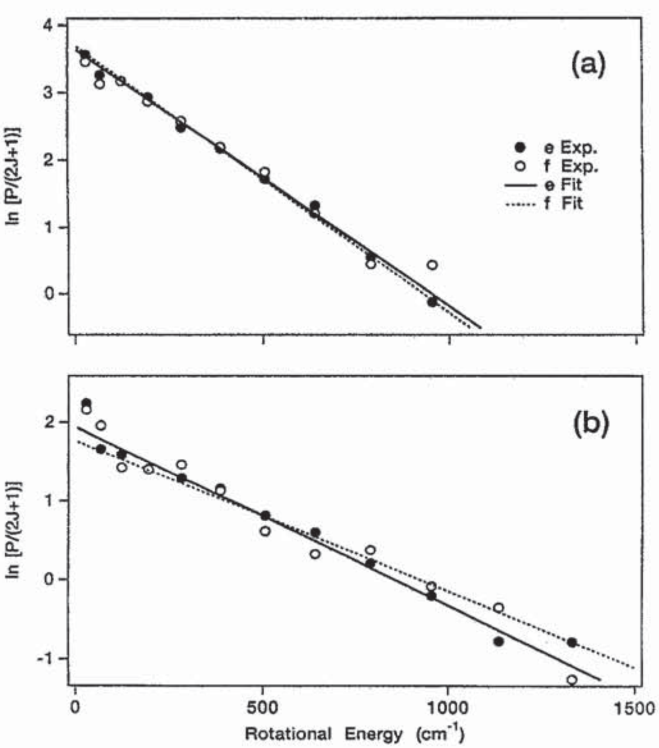

FIG. 11. Boltzmann plots for the product HBr^+ rotational population: (a) HBr^+ ($^2\Pi_{3/2}, v'^+ = 0$) from the reaction DBr^+ ($^2\Pi_{3/2}, v^+ = 0$) + HBr and (b) HBr^+ ($^2\Pi_{3/2}, v'^+ = 0$) from the reaction DBr^+ ($^2\Pi_{1/2}, v^+ = 0$) + HBr. The populations of the *e* and *f* components are fitted separately.

C. Absolute rate constants

The absolute rate constant $k(i,v^+ \to i',v'^+)$ of the charge-transfer channel $(i,v^+) \to (i',v'^+)$ is given by

$$\frac{d\,[HBr^+(i',v'^+)]}{dt} = k(i,v^+ \to i',v'^+) \times [DBr^+(i,v^+)][HBr], \quad (1)$$

where quantities in square brackets represent concentrations. For early times following the initial production of the reagent ion, Eq. (1) can be integrated to yield the expression

$$k(i,v^+ \to i',v'^+) = \frac{[HBr^+(i',v'^+)]}{[HBr][DBr^+(i,v^+)]\Delta t}, \quad (2)$$

where the concentrations $[DBr^+(i,v^+)]$ and [HBr] are assumed constant, and Δt is the time delay between reagent ion formation and product ion measurement. In our experiment, $\Delta t = 400$ ns, and the concentration of HBr is $3.6 \pm 0.4 \times 10^{14}$ molecules cm^{-3}, as measured with a capacitance manometer. Thus, by determining the concentration ratio of $HBr^+(i',v'^+)$ to $DBr^+(i,v^+)$, we evaluate Eq. (2) to find the absolute rate constant.

In what follows, we sum over the rotational levels having the same values of i and v^+ or i' and v'^+ to obtain the relative concentrations $[DBr^+(i,v^+)]$ and $[HBr^+(i',v'^+)]$. Figure 12 illustrates a spectrum covering both DBr^+ and HBr^+ bands under the same conditions. We put the $[DBr^+(i,v^+)]$ and $[HBr^+(i',v'^+)]$ concentrations on the same scale by meeting five conditions: (1) The product ion is normalized in each case to the power of the probe laser and to the total number of reagent ions formed. (2) The absolute transition probabilities[29] for DBr^+ $A\,^2\Sigma^+ - X\,^2\Pi$ and HBr^+ $A\,^2\Sigma^+ - X\,^2\Pi$ are used to convert fluorescence intensities to relative populations. (3) For both HBr^+ and DBr^+ the $A\,^2\Sigma^+\ v = 0$ excited state is the same and has essentially the same radiative lifetime (4.4 μs).[29,30] Consequently, no additional correction is needed to put the two isotopomers on the same footing, assuming that

TABLE II. Rotational temperature of product HBr^+ ($^2\Pi_{i'}, v'^+$).

Channel type	DBr^+ ($^2\Pi_i, v^+$)	HBr^+ ($^2\Pi_{i'}, v'^+$)	Temperature (K)
1	(3/2,0)	(3/2,0)	369 ± 40
1	(1/2,0)	(1/2,0)	371 ± 40
1′	(3/2,1)	(3/2,0)	564 ± 60
1′	(1/2,1)	(1/2,0)	383 ± 120
2	(1/2,0)	(3/2,1)	···
2′	(1/2,0)	(3/2,0)	662 ± 70
2′	(1/2,1)	(3/2,0)	679 ± 70

Downloaded 23 Feb 2012 to 171.64.124.19. Redistribution subject to AIP license or copyright; see http://jcp.aip.org/about/rights_and_permissions

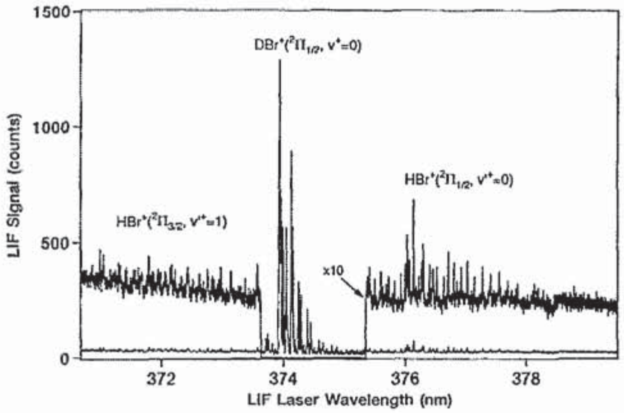

FIG. 12. LIF spectrum of the reagent DBr^+ $A\,^2\Sigma^+ - ^2\Pi_{1/2}$ (0,0) band and the product HBr^+ $A\,^2\Sigma^+ - ^2\Pi_{1/2}$ (0,0) and $A\,^2\Sigma^+ - ^2\Pi_{3/2}$ (0,1) bands. The HBr^+ signal has been expanded by ten times.

quenching processes are also approximately the same. (4) Fluorescence is collected by passing through a narrow-band filter that has a slightly different transmission for each fluorescence band. In addition, the Franck–Condon factors also differ for the HBr^+ A–X and DBr^+ A–X bands. These two effects combine to cause the fluorescence detection efficiency to be 10:17 for HBr^+ compared to DBr^+. A corresponding inverse factor must be applied to place the two concentrations on the same scale. (5) Both DBr^+ and HBr^+ are measured at the same time, $\Delta t = 400$ ns. No correction is made for any possible differential loss of one species compared to the other because the field of view is much larger than the initial volume of DBr that is ionized.

For the $DBr^+(\frac{3}{2},0) \to HBr^+(\frac{3}{2},0)$ charge-transfer channel, $k(\frac{3}{2},0 \to \frac{3}{2},0)$ could be determined at once because the LIF spectra of DBr^+ and HBr^+ are covered by the same laser dye curve. For other channels, we face the problem that different laser dyes are needed to measure the relative populations of $DBr^+(i,v^+)$ and $HBr^+(i',v'^+)$. We lock together all measurements by referencing each set of $HBr^+(i',v'^+)$ product ions recorded with a single laser dye to the total ion signal of $DBr^+(i,v^+)$ recorded by monitoring the ion current using parallel plates (see Fig. 1). In this manner, the absolute rate constants for all channels are determined, and the results are listed in Table III and displayed in Fig. 13. We have also indicated in Table III the undetected product states of DBr and the corresponding energy releases, where a positive number refers to the amount of excess energy available to the products. We estimate that these absolute thermal rate constants have an uncertainty of 20% (one standard deviation) for the stronger charge-transfer channels and a somewhat larger error, as indicated in Table III, for the weaker channels. About half of this uncertainty arises from our absolute measurement of the HBr concentration. Figure 13 clearly illustrates that the largest absolute rate constant is for the nearly resonant charge-transfer channel $DBr^+(\frac{3}{2},0) + HBr(0) \to HBr^+(\frac{3}{2},0) + DBr(0)$. We also observe a strong preference for preserving the spin–orbit component, i.e., $\Delta i = 0$.

IV. DISCUSSION

By laser techniques applied to a gas mixture of HBr and DBr in a bulb we have studied the state-to-state dynamics of the charge-transfer reaction $DBr^+(^2\Pi_i,v^+,J^+) + HBr \to HBr^+(^2\Pi_{i'},v'^+,J'^+) + DBr$. We have also determined the absolute rate constants $k(i,v^+ \to i',v'^+)$ for the different charge-transfer channels. These measurements rely on the ability of (2 + 1) REMPI to prepare DBr^+ ions in nearly pure (i,v^+) states and the ability of LIF to measure the HBr^+ product state distribution as well as the ratio of $HBr^+(i',v'^+)$ to $DBr^+(i,v^+)$.

The interpretation of these results is aided by considering the energetics of the possible charge-transfer channels, shown in Fig. 14. The left-hand side of this figure pictures the four energy levels of the DBr^+ reagent ion accessed in this study; the right-hand side shows the location of the $HBr^+(i',v'^+) + DBr(v')$ product channels. Because of the small change in zero-point energy between HBr and DBr as well as HBr^+ and DBr^+, the following charge-transfer processes are nearly resonant (21 cm^{-1} exoergic): $DBr^+(i=\frac{1}{2},\frac{3}{2};v^+=0) + HBr(v=0) \to HBr^+$

TABLE III. State-to-state thermal absolute rate constants.

Reagent $DBr^+(^2\Pi_i,v^+)$	Product $HBr^+(^2\Pi_{i'},v'^+)$	Rate constant ($\times 10^{-10} cm^3 s^{-1}$)	Product $DBr(v')$	Energy release (cm^{-1})
(3/2,0)	(3/2,0)	4.06 ± 20%	0	21.0
(3/2,1)	(3/2,0)	1.43 ± 20%	1	− 128.2
			0	1711.2
(1/2,0)	(1/2,0)	2.38 ± 20%	0	21.0
	(3/2,1)	0.20 ± 60%	0	325.7
	(3/2,0)	1.19 ± 20%	1	833.1
			0	2672.4
(1/2,1)	(1/2,0)	1.24 ± 20%	1	− 128.2
			0	1711.2
	(3/2,1)	···	1	176.5
			0	2015.8
	(3/2,0)	1.10 ± 30%	2	729.3
			1	2523.2
			0	4362.6

Downloaded 23 Feb 2012 to 171.64.124.19. Redistribution subject to AIP license or copyright; see http://jcp.aip.org/about/rights_and_permissions

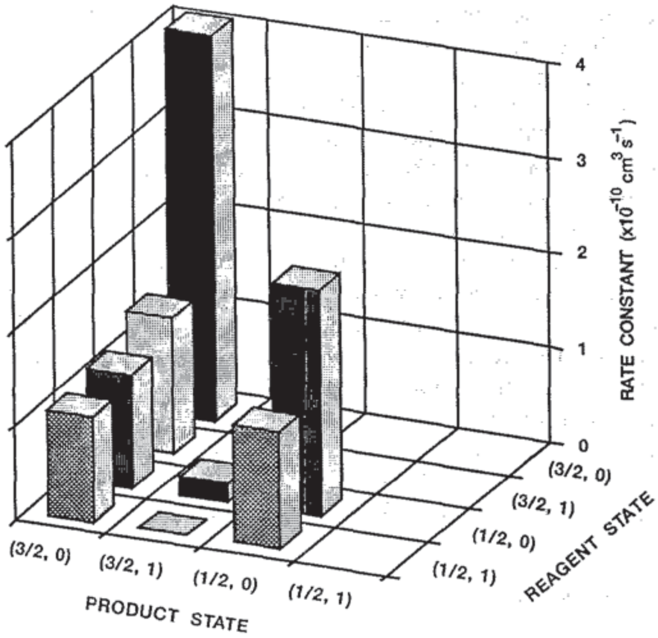

FIG. 13. A 3D diagram of absolute thermal rate constants for the charge-transfer process $DBr^+ + HBr \rightarrow HBr^+ + DBr$, in which the values of the rate constants ($\times 10^{-10}$ $cm^3 s^{-1}$) are plotted along the Z axis, the reagent states along the X axis, and the product states along the Y axis.

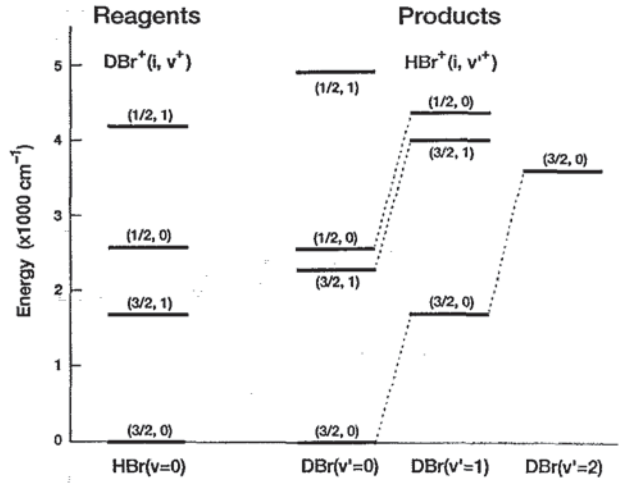

FIG. 14. Energy level diagram of reagents $DBr^+(^2\Pi_i, v^+) + HBr$ and products $HBr^+(^2\Pi_{i'}, v'^+) + DBr$, in which the thick solid lines represent the energy of the two molecules and the dashed lines associate levels with the same $HBr^+(^2\Pi_{i'}, v'^+)$ state but different $DBr(v')$ states.

$\times(i' = \frac{1}{2},\frac{3}{2}; v'^+ = 0) + DBr(v' = 0)$. We call such a nearly resonant channel a type-1 charge-transfer process. In addition, there are several other change-transfer processes, such as $DBr^+(\frac{3}{2},1) + HBr(v = 0)$, that have a nearly resonant channel $HBr^+(\frac{3}{2},0) + DBr(v' = 1)$, as well as off-resonant channels, such as $HBr^+(\frac{3}{2},0) + DBr(v' = 0)$. We call these type-1′ charge-transfer processes. In a similar manner, we denote a charge-transfer process with a single off-resonant channel as a type-2 process, and with more than one such off-resonant channel as a type-2′ process. We have marked in Table III each type of charge-transfer process.

A. Type-1 charge transfer

In a type-1 charge-transfer process, the energy release (21 cm^{-1}) is much less than the thermal energy available (210 cm^{-1}). Examination of Figs. 7(a) and 10 shows that the resulting rotational distributions of the HBr^+ product are slightly warmer than thermal (370 K); see Table II. Because $\Delta i = 0$, $\Delta v^+ = 0$, and $\Delta v = 0$ for these channels, only the conversion between translational and rotational energy occurs. Although the DBr^+ reagent ion is prepared in a narrow distribution of rotational levels, as shown in Fig. 3, the resulting HBr^+ ion reflects closely the HBr thermal rotational distribution. How then can we account for a HBr^+ product rotational distribution that is about 20% hotter than thermal?

The answer to this puzzle leads to a deeper insight into the charge-transfer dynamics than might be first imagined. The standard model is to suppose that the DBr^+ and HBr collision partners form a long-lived complex in which all degrees of freedom are equilibrated. If the DBr^+ reagent ions are assigned a temperature, its value would be close to 50 K. Assuming no dynamical constraints in the separation of the complex, the resulting HBr^+ ions would be expected to have a rotational temperature of approximately 250 K, some 120 K cooler than what is observed. Hence, the charge-transfer process leading to type-1 events must have more complicated dynamics.

Another possibility is in addition to the formation of a long-lived complex, a direct or short-lived charge-transfer process contributes to the type-1 channel. As a first approximation, such a process might be expected to produce HBr^+ ions with a rotational distribution that closely mirrors the HBr reagent (300 K).

Deeper consideration shows that the interaction between the charged DBr^+ and the rotating dipole of HBr may cause some of the translational energy of the reagents to be converted into rotation of the HBr^+ ion. Support for this picture has been provided by Dugan and Magee,[31] who calculated the trajectories for collisions of HCl with a point charge. This interaction may also help to explain why the decomposition of the $DBr^+\cdot HBr$ complex yields rotationally hot HBr^+.

Another possible explanation is the existence of a competing channel for the decomposition of the $DBr^+\cdot HBr$ complex. The formation of $DBrH^+ + Br$ is 0.37 eV exoergic.[32] This mechanism requires that $DBrH^+$ product formation takes place at the expense of colder HBr^+ product ions.

The type-1 channel $DBr^+(\frac{3}{2},0) + HBr(v = 0) \rightarrow HBr^+(\frac{3}{2},0) + DBr(v' = 0)$ has the largest absolute rate among all charge-transfer channels. If we discount small isotope effects, then we expect that half the collisional encounters for this near-resonant process yield HBr^+ ions rather than DBr^+ ions. Consequently, we estimate the total collision rate constant to be $2\times 4.1\times 10^{-10}$ $cm^3 s^{-1}$, which

Downloaded 23 Feb 2012 to 171.64.124.19. Redistribution subject to AIP license or copyright; see http://jcp.aip.org/about/rights_and_permissions

is about 90% of the capture rate constant calculated using the average dipole orientation (ADO) approximation.[16] Thus for this channel the formation of $DBrH^+$ seems to be suppressed.

Recently, Viggiano, Morris, and Paulson[33] have examined the reaction of $H^{79}Br^+$ with DBr in a flowing afterglow and determined the rate constant for $H^{79}Br^+$ disappearance to be 5.3×10^{-10} $cm^3\,s^{-1}$ under thermal conditions (300 K). In this study 20% of the $H^{79}Br^+$ is populated in excited states (vibrational and spin–orbit). By observing the mass-to-charge channels 81–84, Viggiano *et al.* estimate that the absolute rate constant for charge transfer is $2.5\pm0.5\times10^{-10}$ $cm^3\,s^{-1}$ and that for proton transfer is $2.8\pm0.6\times10^{-10}$ $cm^3\,s^{-1}$. If we take our estimates for the rate constants for charge transfer of $DBr^+(i=\frac{3}{2},v^+=0)+HBr$ and $DBr^+(i=\frac{3}{2},v^+=1)+HBr$ and weight them by 4:1 (corresponding to 20% in the first vibrationally excited state), we obtain for DBr^+ a rate constant for charge transfer of $3.5\pm0.7\times10^{-10}$ $cm^3\,s^{-1}$ under the conditions of the experiment of Viggiano *et al.* Thus there is no obvious contradiction between these different measurements, especially when account is taken that different isotopes are involved. Moreover, the total rate of disappearance is comparable to that expected from the (ADO) capture radius. The flowing afterglow experiment of Viggiano *et al.* gives us additional confidence in the validity of our own results.

For the other type-1 process, $DBr^+(\frac{1}{2},0)+HBr(v=0)\rightarrow HBr^+(\frac{1}{2},0)+DBr(v'=0)$, the rate constant is 2.4×10^{-10} $cm^3\,s^{-1}$, corresponding to a total rate constant that is about 60% of the (ADO) capture collision rate constant. This rate constant may be smaller than the other type-1 rate constant because the channels $HBr^+(\frac{3}{2},0)+DBr(v=0,1)$ and $HBr^+(\frac{3}{2},1)+DBr(v'=0)$ may be open. If we take the sum of all such channels, we obtain 4.0×10^{-10} $cm^3\,s^{-1}$, which is nearly the same as the other type-1 collision rate constant.

B. Type-1′ charge transfer

In these charge-transfer processes, DBr^+ is prepared in the internal states $(\frac{3}{2},1)$ and $(\frac{1}{2},1)$ and the HBr^+ product is in the internal states $(\frac{3}{2},0)$ and $(\frac{1}{2},0)$ with the same spin–orbit component as the reagent. The neutral DBr product, however, may be found in $DBr(v'=1)$, which is endoergic by 128 cm^{-1}, and in $DBr(v'=0)$, which is exoergic by 1711.2 cm^{-1}. The former is near resonant with an energy mismatch of less than $kT=210$ cm^{-1}. For $DBr^+(\frac{3}{2},1)+HBr(v=0)\rightarrow HBr^+(\frac{3}{2},0)+DBr(v'=0,1)$, the rotational temperature of the HBr^+ product is 564 K, which is much hotter than the rotational distribution for a type-1 charge-transfer process. We conclude that the near-resonant channel in $DBr^+(\frac{3}{2},1)+HBr(v=0)$ does not make the major contribution to this process. If we assume that the excess energy of 1711.2 cm^{-1} is divided equally among the ten rotational and translational degrees of freedom, the resulting temperature is predicted to be 500 K, in good agreement with what we observe. Again, the calculated temperature is slightly lower (by 64 K); ion–dipole interactions may once more account for this apparent difference. Thus the type-1′ process appears to proceed through a long-lived complex. A simple quantum RRK estimate for the lifetime of the $DBr^+\cdot HBr$ complex is on the order of picoseconds, using the value of about 1 eV for the well depth.[32] This is not sufficient time for vibrational equilibration but statistical behavior may still result in the average over different collision trajectories.

The size of the charge-transfer rate constant (1.43×10^{-10} $cm^3\,s^{-1}$) for $DBr^+(\frac{3}{2},1)+HBr(v=0)\rightarrow HBr^+(\frac{3}{2},0)+DBr(v'=0)$ also indicates that a long-range charge transfer does not occur. Moreover, the smallness of this rate constant may reflect the importance of the competing $DBrH^+ + Br$ product channel. Similar arguments apply to the $DBr^+(\frac{1}{2},0)+HBr(v=0)\rightarrow HBr^+(\frac{1}{2},0)+DBr(v'=0,1)$ charge-transfer channel.

C. Type-2 and type-2′ charge transfer

The $DBr^+(\frac{1}{2},0)+HBr(v=0)\rightarrow HBr^+(\frac{3}{2},1)+DBr\times(v'=0)$ charge-transfer channel is 325 cm^{-1} exoergic. It involves the change of both i and v. Unfortunately, the poor signal-to-noise ratio of our measurements did not allow us to determine a rotational temperature for the HBr^+ product. The absolute rate constant, 0.2×10^{-10} $cm^3\,s^{-1}$, is far smaller than the one for the $DBr^+(\frac{1}{2},0)+HBr(v=0)\rightarrow HBr^+(\frac{1}{2},0)+DBr(v'=0)$ near-resonant channel, in which i does not change. Moreover, it is also smaller than the $DBr^+(\frac{1}{2},0)+HBr(v=0)\rightarrow HBr^+(\frac{3}{2},0)+DBr(v'=0,1)$ off-resonant channel, in which v does not change. Hence we conclude that the simultaneous change of i and v in a charge-transfer process is least preferred.

Actually, our data suggest strongly that the value of v is preserved in a charge-transfer collision in which i changes. We reach this conclusion based on the following calculations. In the $DBr^+(\frac{1}{2},0)+HBr(v=0)\rightarrow HBr^+(\frac{3}{2},0)+DBr(v')$ charge-transfer process, if we assume $v'=0$, then 2672.4 cm^{-1} of energy is released. When this energy is divided equally between the ten rotational and translational degrees of freedom, the resulting temperature is 635 K, which should be compared to our measured temperature of 662 K. Similarly, in the $DBr^+(\frac{1}{2},1)+HBr(v=0)\rightarrow HBr^+(\frac{3}{2},0)+DBr(v')$ charge-transfer process, if we assume $v'=1$, then 2523.2 cm^{-1} of energy is released, leading to a predicted temperature of 616 K. This should be compared to the experimentally determined value of 679 K. In both cases, the predicted temperatures are slightly lower than the measured ones, a discrepancy that might be accounted for by ion–dipole interaction. We also note that the absolute rate constants for these two charge-transfer processes are nearly identical, again suggesting that they proceed by the same mechanism. Thus, we conclude that $\Delta v=0$ is strongly preferred for $\Delta i\neq0$ in $DBr^+ + HBr$ charge-transfer collisions.

Downloaded 23 Feb 2012 to 171.64.124.19. Redistribution subject to AIP license or copyright; see http://jcp.aip.org/about/rights_and_permissions

D. Possible influence of the $DBr^+ + HBr \rightarrow DBrH^+ + Br$ reaction channel

In closing, we note that the absolute charge-transfer thermal rate constants for $DBr^+(\frac{3}{2},0) + HBr$ and $DBr^+(\frac{1}{2},0) + HBr$ are nearly one-half of the rate constant expected in the capture cross section model (ADO approximation). This suggests that the $DBr^+ + HBr \rightarrow DBrH^+ + Br$ reaction does not significantly compete with charge transfer for DBr^+ in the $v = 0$ level, although the $DBrH^+$ product has been observed under thermal conditions by Viggiano *et al.*[33] Table III shows, however, that the absolute charge-transfer rate constants for $DBr^+(\frac{3}{2},1) + HBr$ and $DBr^+(\frac{1}{2},1) + HBr$ are approximately a factor of 2 smaller than the rate constants for DBr^+ in the $v = 0$ level. One explanation for this behavior is that charge transfer from $DBr^+(i,v^+ = 0)$ is more nearly resonant than from $DBr^+(i,v^+ = 1)$. Another explanation is that the $DBr^+ + HBr \rightarrow DBrH^+ + Br$ ion–molecule reaction is promoted by vibrational excitation of the DBr^+ reagent. More work is needed to make a choice between these two possibilities and to assess the importance of the ion–molecule reaction channel in affecting the charge-transfer channel for the $DBr^+ + HBr$ system.

ACKNOWLEDGMENTS

We thank Dr. A. A. Viggiano for making available to us data on the $H^{79}Br^+ + DBr$ reaction prior to publication. Discussions with D. J. Leahy are much appreciated. This work is supported by the U.S. Air Force Office of Scientific Research under Contract No. AFOSR 89-0264.

[1] R. D. Levine and R. B. Bernstein, *Molecular Reaction Dynamics and Chemical Reactivity* (Oxford, New York, 1987).
[2] I. W. M. Smith, *Kinetics and Dynamics of Elementary Gas Reactions* (Butterworths, London, 1980).
[3] D. M. Neumark, A. M. Wodtke, G. N. Robinson, C. C. Hayden, and Y. T. Lee, J. Chem. Phys. **82**, 3045 (1985); D. M. Neumark, A. M. Wodtke, G. N. Robinson, C. C. Hayden, K. Shobatake, R. K. Sparks, T. P. Schafer, and Y. T. Lee, *ibid.* **82**, 3067 (1985).
[4] D. J. Rakestraw, K. G. McKendrick, and R. N. Zare, J. Chem. Phys. **87**, 7341 (1987); R. Zhang, W. J. van der Zande, M. J. Bronikowski, and R. N. Zare, *ibid.* **94**, 2704 (1991).
[5] R. Zhang, D. J. Rakestraw, K. G. McKendrick, and R. N. Zare, J. Chem. Phys. **89**, 6283 (1988); J. G. Pruett and R. N. Zare, *ibid.* **64**, 1774 (1976).
[6] D. A. V. Kliner, D. E. Adelman, and R. N. Zare, J. Chem. Phys. **95**, 1648 (1991).
[7] C. Y. Ng, in *Techniques of Chemistry, Vol. 20, Techniques for the Study of Ion–Molecule Reactions*, edited by J. M. Farrar and W. H. Saunders (Wiley, New York, 1988).
[8] S. L. Anderson, in *Advances in Chemical Physics, State-Selected and State-to-State Ion–Molecule Reaction Dynamics: Experiment, Part I*, edited by C. Y. Ng and M. Baer (in press).
[9] D. Gerlich, in *Advances in Chemical Physics, State-Selected and State-to-State Ion–Molecule Reaction Dynamics: Experiment, Part I*, edited by C. Y. Ng and M. Baer (in press).
[10] W. A. Chupka and M. E. Russell, J. Chem. Phys. **48**, 1527 (1968); W. A. Chupka, in *Ion–Molecule Reactions*, edited by J. L. Franklin (Plenum, New York, 1972).
[11] R. J. S. Morrison, W. E. Conaway, T. Ebata, and R. N. Zare, J. Chem. Phys. **84**, 5527 (1986); W. E. Conaway, T. Ebata, and R. N. Zare, *ibid.* **87**, 3447, 3453 (1987); L. A. Posey, R. D. Guettler, N. J. Kirchner, B. Keller, and R. N. Zare, *ibid.* (to be submitted).
[12] T. M. Orlando, B. Yang, and S. L. Anderson, J. Chem. Phys. **90**, 1577 (1989); T. M. Orlando, B. Yang, Y. Chiu, and S. L. Anderson, *ibid.* **92**, 7356 (1990).
[13] R. N. Zare and P. J. Dagdigian, Science **185**, 739 (1974).
[14] C. E. Hamilton, V. M. Bierbaum, and S. Leone, J. Chem. Phys. **83**, 2284 (1985).
[15] D. M. Sonnenfroh and S. Leone, J. Chem. Phys. **90**, 1677 (1989).
[16] *Gas Phase Ion Chemistry*, edited by M. T. Bowers, Vols. 1 and 2 (1979) and Vol. 3 (1984) (Academic, New York).
[17] D. Gerlich, J. Chem. Phys. **90**, 3574 (1989).
[18] M. Hawley and M. A. Smith, J. Am. Chem. Soc. **111**, 8293 (1989).
[19] D. J. Leahy, J. Xie, and R. N. Zare (unpublished work).
[20] S. L. Anderson, D. M. Rider, and R. N. Zare, Chem. Phys. Lett. **93**, 11 (1982); W. E. Conaway, R. J. S. Morrison, and R. N. Zare, *ibid.* **113**, 429 (1985).
[21] B. G. Koenders, G. J. Kuik, K. E. Drabe, and C. A. De Lange, Chem. Phys. Lett. **147**, 310 (1988).
[22] J. Xie and R. N. Zare, Chem. Phys. Lett. **159**, 399 (1989).
[23] J. M. Brown, J. T. Hougen, K.-P. Huber, J. W. C. Johns, I. Kopp, H. Lefebvre-Brion, A. J. Merer, D. A. Ramsey, J. Rostas, and R. N. Zare, J. Mol. Spectrosc. **55**, 500 (1975).
[24] J. Xie and R. N. Zare (in preparation).
[25] R. Callaghan and R. J. Gordon (to be published).
[26] I. Kopp and J. T. Hougen, Can. J. Phys. **45**, 1581 (1967).
[27] L. T. Earls, Phys. Rev. **48**, 423 (1935).
[28] J. Lebreton, J. Chim. Phys. **70**, 1188 (1973).
[29] G. R. Mohlmann and F. J. De Heer, Chem. Phys. **17**, 147 (1976).
[30] C. C. Martner, J. Pfaff, N. H. Rosenbaum, A. O'Keefe, and R. J. Saykally, J. Chem. Phys. **78**, 7073 (1983).
[31] J. V. Dugan, Jr. and J. L. Magee, J. Chem. Phys. **47**, 3103 (1967).
[32] P. W. Tiedemann, S. L. Anderson, S. T. Ceyer, T. Hirooka, C. Y. Ng, B. H. Mahan, and Y. T. Lee, J. Chem. Phys. **71**, 605 (1979).
[33] A. A. Viggiano, R. A. Morris, and J. F. Paulson (unpublished data).

Downloaded 23 Feb 2012 to 171.64.124.19. Redistribution subject to AIP license or copyright; see http://jcp.aip.org/about/rights_and_permissions